Synthetic and Systems Biotechnology 10 (2025) 294–306

Contents lists available at ScienceDirect

Synthetic and Systems Biotechnology

journal homepage: www.keaipublishing.com/en/journals/synthetic-and-systems-biotechnology

Original Research Article

Semi-rational design and modification of phosphoketolase to improve the yield of tyrosol in *Saccharomyces cerevisiae*

Na Song [a,1], Huili Xia [b,1], Yaoru Xie [a], Shuaikang Guo [a], Rong Zhou [a], Lingling Shangguan [a], Kun Zhuang [a,c], Huiyan Zhang [a], Feiran An [a], Xueyun Zheng [a], Lan Yao [a], Shihui Yang [d], Xiong Chen [a,**], Jun Dai [a,d,*]

[a] *Cooperative Innovation Center of Industrial Fermentation (Ministry of Education & Hubei Province), Key Laboratory of Fermentation Engineering (Ministry of Education), National "111" Center for Cellular Regulation and Molecular Pharmaceutics, Hubei Key Laboratory of Industrial Microbiology, School of Life and Health Sciences, Hubei University of Technology, Wuhan, Hubei, 430068, PR China*

[b] *College of Biological and Food Engineering, Huanghuai University, Zhumadian, 463000, PR China*

[c] *School of Food Science and Engineering, Wuhan Polytechnic University, Wuhan, 430023, PR China*

[d] *State Key Laboratory of Biocatalysis and Enzyme Engineering, School of Life Sciences, Hubei University, Wuhan, Hubei, 430062, PR China*

ARTICLE INFO

Keywords:
Tyrosol
D-Erythrose 4-phosphate
Phosphoketolase
PHK pathway

ABSTRACT

Tyrosol is an important component of pharmaceuticals, nutraceuticals, and cosmetics, and their biosynthetic pathways are currently a hot research topic. D-Erythrose 4-phosphate is a key precursor for the biosynthesis of tyrosol in *Saccharomyces cerevisiae*. Hence, the flux of D-Erythrose 4-phosphate determined the yield of tyrosol synthesis. In this study, we first obtained an *S. cerevisiae* strain S19 with a tyrosol yield of 247.66 mg/L by metabolic engineering strategy. To increase the production of D-Erythrose 4-phosphate, highly active phosphoketolase BA-C was obtained by bioinformatics combined with tyrosol yield assay. The key residue sites 183, 217, and 320 were obtained by molecular docking, kinetic simulation, and tyrosol yield verification. After mutation, the highly efficient phosphoketolase BA-C^{His320Met} was obtained, with a 37.32 % increase in enzyme activity. The tyrosol production of strain S26 with BA-C^{His320Arg} increased by 43.05 % than strain S25 with BA-C and increased by 151.19 % compared with the strain S19 without phosphoketolase in a 20 L fermenter. The mining and modification of phosphoketolase will provide strong support for the de novo synthesis of aromatic compounds.

1. Introduction

Tyrosol as a phenethyl alcohol derivative, possesses notable antioxidant and anti-inflammatory properties [1]. Tyrosol is also a crucial pharmaceutical intermediate such as salidroside, icariside D2, and hydroxytyrosol, which are known for their efficacy against cardiovascular disease, cancer, and viruses [2–5]. Tyrosol can be extracted directly from plants such as olives, but its yield is low due to the limitation of cultivated land and climate [6]. In addition, chemical synthesis methods pose a great threat to the environment, and tyrosol precursors are often expensive [7–9]. With the development of synthetic biology, tyrosol can be synthesized in *Escherichia coli, and S. cerevisiae* [10–14]. The biosynthesis method is environmentally friendly, has low energy consumption, and its production method is efficient and easy to operate [15].

S. cerevisiae has been widely used as a microbial cell factory in industrial biotechnology due to its safety, high fermentation efficiency, and robustness to harsh fermentation conditions [16]. It has been demonstrated that tyrosol was natively biosynthesized in *S. cerevisiae* via the Ehrlich pathway [4]. Under the action of *ARO10*, 4-hydroxyphenylpyruvate (4-HPP) was converted into 4-hydroxyphenylacetic acid (4-HPAA), and then tyrosol was produced under the action of alcohol

Peer review under the responsibility of Editorial Board of Synthetic and Systems Biotechnology.

* Corresponding author. School of life and health sciences, Hubei University of Technology, No. 28, Nanli Road, Hongshan District, Wuhan, Hubei, 430068, PR China.

** Corresponding author. School of life and health sciences, Hubei University of Technology, No. 28, Nanli Road, Hongshan District, Wuhan, Hubei, 430068, PR China.

E-mail addresses: cx163_qx@163.com (X. Chen), jundai@hbut.edu.cn (J. Dai).

[1] These authors have contributed equally to this work and share the first authorship.

https://doi.org/10.1016/j.synbio.2024.11.007
Received 22 August 2024; Received in revised form 23 November 2024; Accepted 25 November 2024
Available online 26 November 2024

dehydrogenases (ADHs) [3,17]. At present, the production of tyrosol in *S. cerevisiae* has been greatly improved through various metabolic engineering strategies. Constructed heterologous pathway using the gene $TYRA^{M53I/A354V}$ encoding a bifunctional NAD^+-dependent fused chorismate mutase/prephenate dehydrogenase from *Escherichia coli* and gene *AAS* encoding aromatic aldehyde synthase obtained from *Petroselinum crispum* to enhance the synthesis of tyrosol [13,14]. Deleted the pyruvate decarboxylase gene *PDC1* to redirect the flux distribution at the pyruvate node and restrained the biosynthetic pathways of L-phenylalanine and L-tryptophan by disrupting prephenate dehydratase PHA2 and bifunctional anthranilate synthase TRP3 [12,18]. Introduced the mutation $ARO3^{D154N}$ to relieve the feedback inhibition of L-phenylalanine resulting in the tyrosol reaching 1.3 g/L [19]. Overexpressed chorismite (CHA) synthase and chorismate mutase to maximize the aromatic amino acid flux towards tyrosol synthesis [20]. However, D-Erythrose 4-phosphate (E4P) synthesis is a key rate-limiting step in the de novo synthesis of tyrosol by *S. cerevisiae* [18]. It has been demonstrated that the available carbon flux of E4P was at least one order of magnitude lower than that of phosphoenolpyruvate (PEP) even in strains with optimized initial productivity of aromatic amino acid (AAA) pathway [21,22].

To address the possible constraints on the entrance flux into the E4P biosynthetic pathway, previous studies focused on rewiring the pentose phosphate pathway (PP pathway). This includes overexpression of transketolase TKL1, deletion of glucose-6-phosphate dehydrogenase ZWF1, transaldolase TAL1, and modified ribose-5-phosphate ketol-isomerase RKI1 [23–25]. However, none of these strategies could efficiently divert carbon flux from glycolysis toward E4P, to provide sufficient levels for biosynthesis of aromatic chemicals. Recent studies show that rewiring the central carbon metabolism by constructing a heterologous phosphoketolase (PHK) pathway in cells was efficient in providing E4P and channels more flux through the AAA biosynthesis pathway [12,18,26,27]. The PHK pathway consists of a phosphoketolase and a phosphotransacetylase (PTA). Phosphoketolase catalyzes the conversion of fructose-6-phosphate into E4P and acetyl-phosphate (AcP) (Fig. 1). Guo et al. expressed phosphoketolase in *S. cerevisiae*, the carbon flux of the Xfpk-based pathway was twice as high as that of the PP pathway in theory, further confirming that the Xfpk-based pathway was a more conducive pathway for the precursor E4P supply for the shikimate pathway [12]. It may further facilitate the biosynthesis of aromatic amino acids and the production of tyrosol in *S. cerevisiae*. Although the above studies have confirmed the effectiveness of phosphoketolase in tyrosol production, the activity of phosphoketolase does not meet the application and demand of biosynthesis.

Thanks to the rapid advancements in high-throughput sequencing technologies, vast amounts of nucleotide and protein data from various samples have been sequenced and deposited in public databases. From these databases, a wealth of enzymes can be mined, which in turn are applied to biocatalysis and metabolic engineering [28]. The fast development of bioinformatics tools for the accurate prediction of protein structures facilitated the understanding and rational engineering of proteins [29]. Three-dimensional structures, key amino acid residues in protein obtained by molecular docking, and kinetic simulation can be selected for rational or semi-rational mutations to tune their

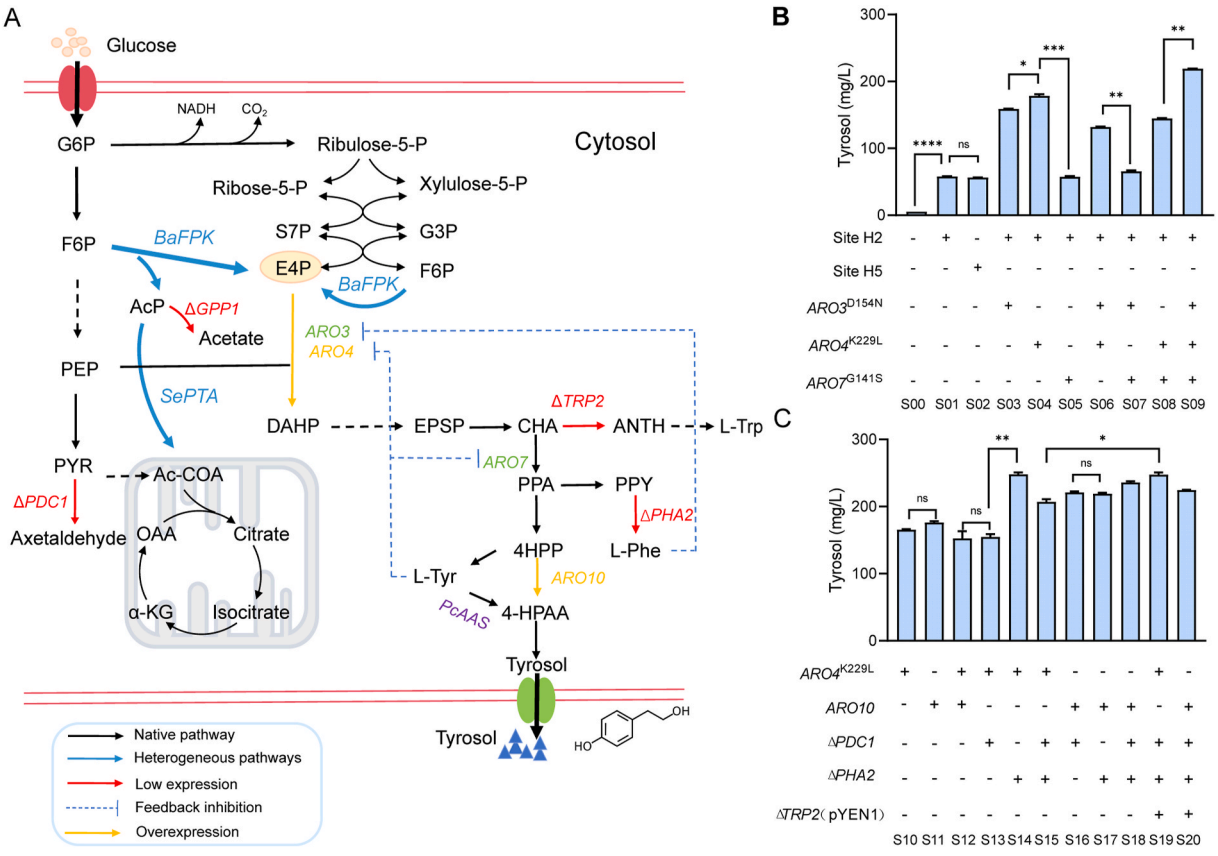

Fig. 1. Metabolic engineering modification of the tyrosol synthesis pathway in *S. cerevisiae*. (A) Strategies for modifying the synthetic and metabolic pathways of tyrosol in *S. cerevisiae*. (B) Heterologous expression of *PcAAS* and elimination of amino acid feedback inhibition. (C) The overexpression of *ARO4* and *ARO10* and the knock-out of branching pathways. Metabolite abbreviations: G6P: Glucose 6-phosphate; Ribulose-5-P: D-Ribulose 5- phosphate; Xylulose-5-P: D-Xylulose 5-phosphate; Ribose-5-P: D-Ribose 5-phosphate; S7P: Sedoheptulose 7-phosphate; G3P: D-Glyceraldehyde 3-phosphate; F6P: beta-D-Fructose 6-phosphate; PEP: phosphoenolpyruvate; E4P: D-Erythrose 4-phosphate; PYR: pyruvic acid; DAHP: 3-deoxy-D-arabino-heptulosonate-7-phosphate; EPSP: 5-enolpyruvyl-3-shikimate; CHA: chorismate; ANTH: anthranilate; PPA: prephenate; PPY: phenylpyruvate; 4-HPP: 4-hydroxyphenylpyruvate; 4-HPAA: 4-hydroxyphenylacetic acid; L-tyr: L-tyrosine; L-Phe: L-phenylalanine; L-Trp: L-tryptophan; AcP: acetylphosphate; Ac-COA: acetyl coenzyme A; OAA: oxaloacetate; α-KG: Alpha ketoglutaric acid.

characteristics [30–32]. Xu et al. conducted protein engineering of pyruvate decarboxylase from *Candida tropicalis* (*Ct*PDC) to improve decarboxylation efficiency, *CtPDC*^{Mu5} caused the tyrosol yield to reach 38 g/L with 99.6 % conversion [33]. Qu et al. performed the interaction fingerprinting analysis of carboxylic acid reductase (CAR) with ligand and identified 17 residues at the substrate binding pockets, after single site saturation mutagenesis the variants were successfully obtained. As a result, the conversion of mutant K524W was a 2-fold improvement compared to the wild-type [34].

In this study, through the implementation of a metabolic engineering strategy, we successfully engineered a strain capable of producing a quantifiable amount of tyrosol. Screening out a highly active phosphoketolase BA-C from *Bifidobacterium asteroides* through big data mining and experimental verification. Through docking with substrate molecules and kinetic simulations, we identified critical residue sites of BA-C. For the screened sites, we conducted virtual mutation predictions. A highly active phosphoketolase mutant BA-C^{His320Arg} was obtained. The mutant phosphoketolase increased the yield of *S. cerevisiae* by 43.05 % in a 20 L fermentor. These efforts provide potential insights for the rational modification of enzymatic activity.

2. Materials and methods

2.1. Strains construction and cultivations

The *S. cerevisiae* strains constructed in this paper are listed in Supplementary Data 1. The plasmids used in this study were listed in Supplementary Data 3 and the primers were listed in Supplementary Data 4. The DNA sequences of heterologous genes were obtained from NCBI. The heterologous genes were synthesized by Sangon Biotech, China. All the sequences were listed in Supplementary Data 6. The information on insertion sites and homologous arms is shown in Supplementary Data 5, and the structure of homologous arms and shown in Supplementary Data 2. SC-Ura medium containing 20 g/L Dextrose, 6.7 g/L Yeast nitrogen base (with Ammonium sulfate, without Amion acids), 1.29 g/L Do supplement-Ura was used for yeast transformation, yeast strains containing pYES2 plasmid were cultured in SC-Ura medium which replace dextrose with 2 % galactose and 1 % raffinose. The other yeast was cultured in YEPD medium containing 20 g/L Peptone, 10 g/L Yeast extract, and 20 g/L Dextrose. *E. coli* was cultured in an LB medium containing 5 g/L Yeast extract, 10 g/L Peptone, and 10 g/L NaCl, pH 7.2.

Yeast strains were picked from a strain preservation tube and cultured in 5 mL YPD medium at 30 °C, shaking at 200 rpm for 24 h. Portions of the pre-cultured mixture were then transferred into 50 mL YPD medium in 250 mL shake flasks until the OD_{600} value reached approximately 0.5. The strains were cultured at 30 °C, shaking at 200 rpm for 72 h. To monitor the growth of cells, we used a spectrophotometer to measure the samples at different times of fermentation at 600 nm. Samples were collected and centrifuged at 12000 rpm for 3 min. The supernatant was stored at −20 °C until analysis.

2.2. Sequence alignment and phylogenetic analysis

Using the xfpk_Bb sequence as a template, the blast was performed in NCBI (https://blast.ncbi.nlm.nih.gov/Blast.cgi) and then clustered using Cdhit with a threshold for dereplication at 73 % (https://www.bioinformatics.org/cd-hit/). The phylogenetic tree construction using MEGA11 with the maximum likelihood method (https://www.megasoftware.net/) [35]. The obtained phylogenetic tree was optimized using the online software Interactive Tree of Life (https://itol.embl.de/). All phosphoketolase enzyme-related information can be seen in Supplementary Data 7.

2.3. In vitro phosphoketolase activity assay

Strains were cultivated in biological duplicates in 100 mL SC media for 24 h. The cells were harvested by centrifugation, washed twice with 15 mL of TEK buffer containing 50 mM Tris-HCl, 1 mM EDTA, and 100 mM potassium chloride (pH 7.4), and the cell pellet was resuspended in 1 mL lysis buffer containing 50 mM NaH_2PO_4, 3 mM NaCl, and 1 mM PMSF (pH 7.4). All procedures were performed on ice with chilled solutions. The cell suspension was transferred to a pre-chilled tube with 0.5 mm glass beads and homogenized using a TGrinder H24R tissue homogenizer (TIANGEN, TIANGEN BIOTECH (BEIJING) Co., LTD., Beijing, China) (4 °C, 3600 rpm for 30 s, 15 s resting, 10 cycles). The homogenized mixture was centrifuged (4 °C, 12000 rpm, 20 min), and the crude cell-free extract was stored on ice. Protein concentrations were determined with an RC DC™ Protein Assay (Bio-Rad Laboratories, Inc., California, USA) using bovine serum albumin standards.

Reactions were carried out in 96-well microtiter plates in a total volume of 100 μL containing 90 μL enzyme buffer and either the substrate R5P (50 mM) or F6P (50 mM). The enzyme buffer contains 50 mM Tris (pH 7.5), 5 mM $MgCl_2$, 5 mM potassium phosphate, and 1 mM thiamine pyrophosphate. The crude cell-free extract (10 μL) was added to start the reaction. The reactions were incubated at 30 °C for 30 min, 60 min, 90 min, and 120 min, after which 75 μL NH_2OH–HCl (2 M, pH 6.5) was added to stop the enzymatic reaction. 10 min later, 50 μL each of Cl_3CCOOH (0.92 M), HCl (4 M), and $FeCl_3$ (0.185 M in 0.1 M HCl) was added to each reaction to generate ferric hydroxamate, which is brown and was measured at 505 nm. Commercial lithium potassium AcP was used to relate absorbance to concentration; the standard curve showed a linear relationship between 0 and 15 mM in the conditions described [36].

2.4. Site-specific mutagenesis

The phosphoketolase genes were integrated into the pYES2 plasmid and expressed by induction of galactose in yeast. Site-specific mutation was performed using Mut Express II Fast Mutagenesis Kit V2 (Vazyme Biotech Co., Ltd., Nanjing, China). The method was based on ClonExpress homologous recombination technology (Fig. S1). The original plasmid was first reverse-amplified by introducing mutated primers, and then the amplified product was digested using *Dpn*I. Finally, the recombinant reaction was catalyzed by the enzyme Exnase II, and then converted to *E. coli* DH5α, the positive clones were selected.

2.5. DNA manipulations

The CRISPR-Cas9 system was applied to modify the genome. Plasmid pML104 was used to construct gRNA expression vectors [37]. The specific guide RNA sequences were designed using the CHOPCHOP web tool [38] (http://crispor.tefor.net). To construct homologous recombination fragments, the plasmid pTEF1-CYC1 and pADH1-CYC1 were firstly linearized using restriction enzymes, and phosphoketolases fragments were ligated together through ClonExpress MultiS One Step Cloning Kit (Vazyme Biotech Co., Ltd., Nanjing, China) (Fig. S2). In the same way, the upstream and downstream homologous arms of the insertion site were added to the plasmid constructed in the previous step. The gRNA expression vectors and homologous recombination fragments were co-converted into yeast by the LiAc/ssDNA/PEG method [39]. The corrected yeast clones were selected on SC-Ura medium.

2.6. Molecular docking and dynamics simulation

Homology modeling was carried out using SWISS-MODEL (https://swissmodel.expasy.org/). The chemical structures of compounds were retrieved from the PubChem database (http://pubchem.ncbi.nlm.nih.gov/), and energy minimization of phosphoketolase was carried out using Chem3D (https://library.bath.ac.uk/chemistry-software/chem3d). Molecular docking is done by the Glide module in Schrödinger Maestro software (Schrödinger, Inc., New York, USA). Protein processing utilizes the Protein Preparation Wizard module.

The molecular docking simulations were carried out using AMBER18 (https://ambermd.org/AmberTools.php). The protein and the substrate were parameterized with the Amber ff14SB force field and the GAFF2 force field, respectively, while the complex was solvated in a cuboid box with a 12 Å buffer of TIP3P water molecules. Antechamber (https://ambermd.org/antechamber/ac.html) was adopted to generate the parameters of the ligand. The system was neutralized by adding Na^+. The steepest descent method and conjugate gradient method were used to minimize the energy in two steps to eliminate the bad contact of atoms in the system. Then the system was slowly heated from 0 K to 300 K within 50 ps under the weak restraint of 10 kcal/mol/$Å^2$. The SHAKE algorithm was used to constrain chemical bonds involving hydrogen atoms. At last, a 100 ns molecular docking simulation was carried out under the restraint of constant temperature and pressure. Atomic trajectories were analyzed using Schrödinger Maestro to generate RMSF, RMSD, and distances between specified atoms.

2.7. Amino acid mutation prediction

The phosphoketolase BA-C was treated using the Protein Preparation Wizard module. Receptors are preprocessed, optimized, and minimized (constraint minimization using OPLS3e force fields). Schrödinger 2019.01 Residue Scanning and Mutate Building modules were used for protein mutation scanning and mutate building, respectively. Firstly, Protein Preparation was used to pretreat the protein to remove excess water molecules, add missing hydrogen atoms, repair missing bond information, and repair missing peptides. Then, the small molecules are pretreated and hydrogenated using the LigPrep module. Then we confirm the active site, import the processed protein, use the Binding Site Detection module to predict the protein site, and use it as the center of mass of the 12 Å × 12 Å × 12 Å box to confirm the site grid file. Finally, molecular docking analysis was performed by Ligand Docking.

2.8. Analytical methods

Tyrosol was determined by high-performance liquid chromatography (HPLC). Thermo-C18 column (4.6 mm × 250 mm, 5 μm) was used. Detection conditions: Mobile phase containing 0.05 % (v/v) formic acid aqueous solution (A) and acetonitrile (B), gradient elution (0–20 min, 20 % B; 20–25 min, 95 % B; 25–35 min, 95 % B; 35–40 min 95 % B; 40 min–50 min 10 % B), column temperature was 30 °C, flow rate was 1 mL/min, detection wavelength was 224 nm.

2.9. Fed-batch fermentation for tyrosol production

Seed cultures of 1L were transferred into 20 L bioreactors (Shanghai Baoxing Bio-Engineering Equipment Co., Ltd., Shanghai, China) containing 14 L fed-batch medium (20 g/L peptone, 20 g/L yeast extract, and 20 g/L glucose) when the OD_{600} of seed cultures reached 5. Fermentation was performed at 30 °C; pH was maintained at 5.7 by automated addition of 5 M NaOH. Air flow was set at 2.5 vvm (air volume/working volume min^{-1}) and the dissolved oxygen (dO2) concentration was controlled above 40 % saturation by agitation cascade (400–600 rpm). Glucose solution (600 g/L) was fed periodically into the fermentation system to maintain the glucose concentration under 5 g/L. The feeding time starts from the 12th hour of fermentation to the end of the 60th hour. Regular feeding, adding a certain amount of glucose solution at a rate of 3 g/L per hour. Batch feeding control is shown in Table S2. Cell density, glucose, and ethanol concentration were constantly monitored during the fermentation process. One milliliter supernatant of fermentation cultures was stored every 4 h at −20 °C until analysis.

2.10. Data analysis

Heat maps, scatter graphs, and bar graphs were made using Prism software (GraphPad Prism 8.0.2, San Diego, CA, USA). Error bars represent standard deviation. $P < 0.05$ (n = 3) indicated a significant difference. Significance is indicated by an asterisk. The significance level determination was calculated by T-test and single factor analysis of variance (ANOVA). The curve of AcP is obtained by nonlinear fitting.

3. Results

3.1. Metabolic engineering modification of the tyrosol synthesis pathway in S. cerevisiae

To augment the production of tyrosol, we reengineered the Ehrlich pathway in *S. cerevisiae* CEN.PK113-5D by introducing heterologous *PcAAS*, which can transform L-tyrosine into 4-hydroxyphenylacetic acid (4-HPAA). 4-HPAA was synthesized concurrently through an artificial pathway and the yeast's natural tyrosol biosynthetic pathway (Fig. 1A). The heterologous *PcAAS* gene was successfully integrated into the loci of H2 and H5 in the *S. cerevisiae* CEN.PK113-5D (S00), generating strain S01 and S02, respectively [40]. As shown in Fig. 1B, the tyrosol titer of strain S01 was 57.68 mg/L, which was 74.9 fold than that of S00. The tyrosol titer of strain S02 was 55.44 mg/L, which was 10.24 times that of strain S00. These results indicated that both of these loci exhibited high expression levels of the *PcAAS* gene.

To relieve the feedback inhibition of L-tyrosine on *ARO4* and *ARO7* and L-phenylalanine on *ARO3*. The in situ $ARO3^{D154N}$, $ARO4^{K229L}$ and $ARO7^{G141S}$ mutations were performed in *S. cerevisiae* S01 using the Crispr-Cas9 system (Fig. 1B). The yields of tyrosol after mutating *ARO3*, *ARO4* and *ARO7* were 158.29 mg/L, 178.59 mg/L, and 57.57 mg/L, respectively. However, both mutant *ARO3* and *ARO4* or *ARO4* and *ARO7* had lower tyrosol yields than mutant *ARO3* and *ARO4* alone. The yield of tyrosol both mutated *ARO3* and *ARO7* was 65.57 mg/L. According to the results, we speculated that *ARO3* and *ARO4* played a major role in relieving feedback inhibition compared with *ARO7* [41]. Interestingly, fluorescence quantitative results also showed that the expression of *ARO4* of strain S09 compared with S08 was significantly increased (Fig. S3). The expression of the *ARO4* gene is regulated by transcriptional GCN4p, and this regulation is related to the change in amino acid content [42,43]. The simultaneous mutation of *ARO3*, *ARO4*, and *ARO7* generated strain S09, which exhibited a tyrosol yield of 219.03 mg/L, marking a significant 3.79-fold increase compared to that of the strain S01. These results suggest that the simultaneous release of feedback inhibition of *ARO3*, *ARO4*, and *ARO7* would be more conducive to tyrosol production.

To further increase tyrosol production, a copy of $ARO4^{K229L}$ with strong constitutive promoters was introduced into the *delt* locus of S09. However, the overexpression of endogenous $ARO4^{K229L}$ and *ARO10* could not lead to higher titers of tyrosol in strain S10 (165.54 mg/L) and S11 (176.39 mg/L) (Fig. 1C). The results could be attributed to two plausible reasons: (1) the diversion of PEP to PYR leads to the reduction of DHAP production; (2) the diversion of chorismic acid to the production of L-phenylalanine and L-tryptophan [44]. To validate our hypothesis, we would knock out the key genes involved in the three branches based on the aforementioned engineered strains.

PDC1 was one of the main enzymes of the three pyruvate decarboxylases (PDC1, PDC5, and PDC6), catalyzed the process of decarboxylating pyruvate to acetaldehyde, competing with the accumulation of PEP and E4P [45]. When the *PDC1* gene was disrupted, it led to a significant reduction in overall pyruvate decarboxylase activity by approximately 30 % and increased the production of aromatic compounds in *S. cerevisiae* [46]. Therefore, *PDC1* was disrupted in strains S10 and S11, generating strains S13 and S16, with a tyrosol yield of 154.84 mg/L and 221.11 mg/L (Fig. 1C). In strain S16, the ethanol production decreased significantly at 60 h (Fig. S4) and the yield of tyrosol increased by 42.79 % compared to that of strain S11. The result suggested that the elimination of *PDC1* based on *ARO10* overexpression strain contributed to the increase of tyrosol (Fig. 1C). However, tyrosol

did not increase in the strain that overexpressed *ARO4*, which further indicated that there might be an obvious competitive pathway for tyrosol production.

As CHA serves as a precursor to the biosynthesis of L-tryptophan, L-phenylalanine, and L-tyrosine, to reduce the flux of CHA to L-tryptophan and L-phenylalanine, *PHA2* was knocked out separately in strain S10 and S11 (Fig. 1C), yielding strains S14 and S17. Strain S14 accumulated 248.03 mg/L tyrosol, which was 49.83 % greater than that of strain S10, and the content of phenylethanol decreased obviously (Fig. S5A). The yield of tyrosol reached 236.13 mg/L after the elimination of *PHA2* and *PDC1* in strain S18. This result indicated that the synthesis of phenylalanine was one of the main branching pathways of CHA. To further increase the flow of CHA to prephenate (PPA), the branch to tryptophan also could be knocked out. However, the deletion of the *TRP2* gene cause significant growth deficiency [23]. The expression of the *TRP2* gene was downregulated through the replacement of the original promoter of gene *TRP2* with a weak promoter *YEN1* yielding strains S19 and S20, with a yield of 247.66 mg/L and 224.54 mg/L, respectively. The tyrosol yield of strain S19 was increased by 19.64 % compared to strain S15. The content of tryptophol in strains S19 and S20 also decreased accordingly (Fig. S5B). In summary, these metabolic engineering operations have led to a gradual increase in tyrosol production, but the production is far from reaching a high level. Hence, the DAHP generation step is still a bottleneck, and next step we will build the PHK pathway and further increase DAHP generation.

3.2. Phosphoketolase protein sequence analysis

To mine phosphoketolase enzymes with high activity, we first used the amino acid sequence of phosphoketolase from *Bifidobacterium breve* (xfpk_BB, sequence ID: KND53308.1) and *Bifidobacterium lactis* (xfpk_BL, sequence ID: AJD88698.1) as a template for BLAST comparison with the Nr database (Table S1). In previous studies, xfpk_BL and xfpk_BB have high enzyme activity in *S. cerevisiae* [27]. After comparison, we obtained approximately 40,000 sequences. Then, 280 sequences with conserved sites (metal ion binding sites; residues around the substrate binding bag) were preserved. The phylogenetic tree was constructed by the maximum likelihood method using the above 280 screened phosphoketolase sequences and 9 phosphoketolase sequences that have been reported to be active in *S. cerevisiae*. As shown in Fig. 2, these phosphoketolases in the phylogenetic tree are derived from 24 phyla, primarily from the Actinobacteria, Proteobacteria, Chlorobi, and Firmicutes. Proteobacteria, Firmicutes, and Actinobacteria are the most abundant natural bacterial phyla currently reported, indicating that phosphoketolase derived from these phyla has a relatively complete evolutionary history [47,48]. The nine active phosphoketolases initially selected are primarily from the Actinobacteria and Firmicutes. For further study, the EFE89336.1 from *Bifidobacterium breve* and WP_144085670.1 from *Bifidobacterium asteroides* which closely related to the template from the constructed phylogenetic tree were selected, and they were designated BA-C and BB-D, respectively [27]. The xfpk_BB and xfpk_BL were also synthesized after codon optimization as a comparison, all of them come from Actinobacteria (Table S1).

3.3. Activity and substrate specificity of phosphoketolase in S. cerevisiae

To investigate the activity of these enzymes which screened from phylogenetic analysis in *S. cerevisiae*. The plasmid pYES2 was used to

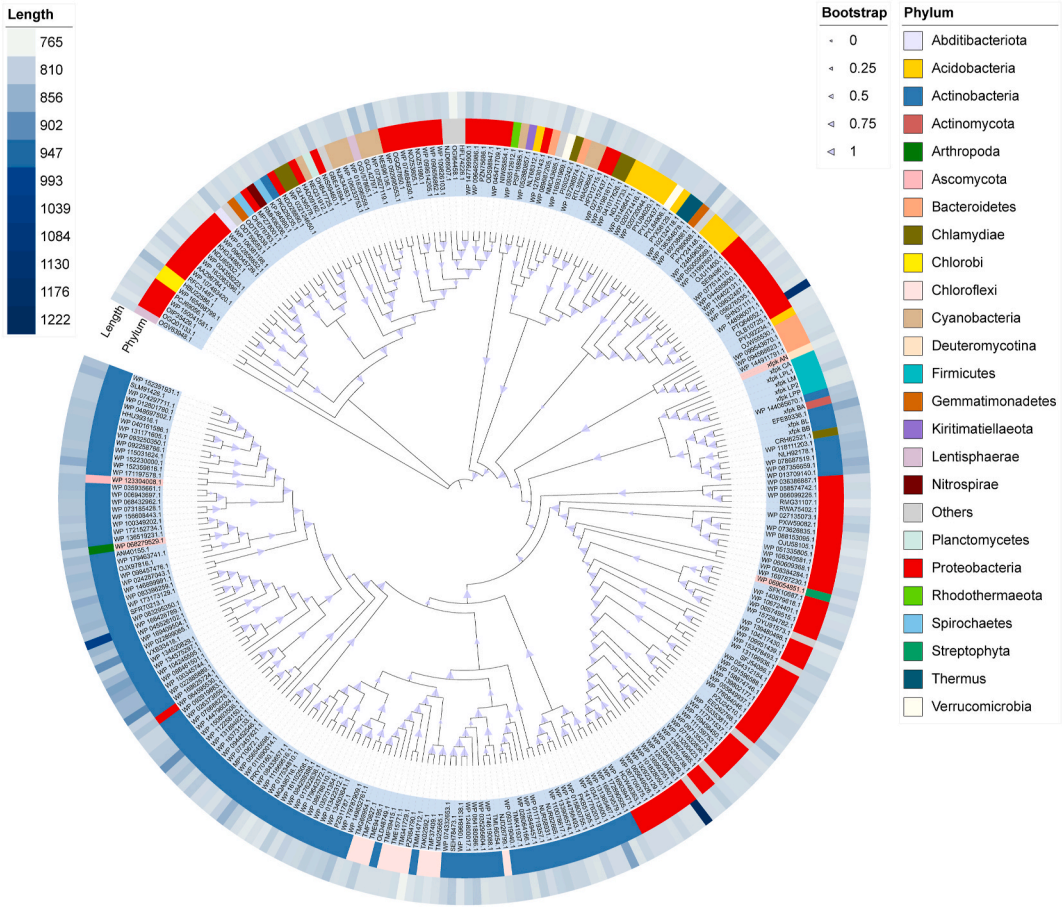

Fig. 2. Phylogenetic analysis of phosphoketolases. The MEGA 11 software were used for the sequence alignment and construction of the phylogenetic tree using the full-length sequences of 289 phosphoketolases.

express these phosphoketolases in *S. cerevisiae* S19 generating strains S19-xfpk_BB, S19-xfpk_BL, S19-BA-C, and S19-BB-D (Fig. 3A). These strains were cultured in a SC medium containing 2 % galactose. The tyrosol production of S19-xfpk_BB and S19-BA-C were 348.92 mg/L and 380.64 mg/L, which increased by 42.04 % and 55.49 % than that of strain S19 with pYES2 empty plasmid, respectively. Although S19-BB-D is also derived from the same *B. breve* as S19-xfpk_BB, the yield of S19-xfpk_BL and S19-BB-D were average. Therefore, the S19-BA-C was chosen to continue the study.

To reveal the functional expression and substrate specificity of BA-C, an *in vitro* enzyme assay was performed with crude cell extracts from *S. cerevisiae* S19- pYES2 and *S. cerevisiae* S19-BA-C based on the established ferric hydroxamate method. Phosphoketolase has bifunctional properties, which catalyze the conversion of F6P to E4P and AcP, and catalyze xylulose-5-phosphate (X5P) to glyceraldehydes-3-phosphate (G3P) and AcP (Fig. S6). According to previous studies, ribose-5-phosphate (R5P) could be used as a substitute for natural substrate X5P. The catalytic function of phosphoketolase enzyme to substrates F6P and R5P was determined by detecting the amount of AcP [49]. As shown in Fig. 3B and C, the total time of the enzymatic reaction was 120 min, group C was the crude enzyme extract of S19- pYES2, and group T was the crude enzyme extract of S19-BA-C. When the enzymatic reaction was carried out for 60 min, the Acp production of group C and group T was 3.14 mM and 5.03 mM, respectively, when F6P was used as substrate. When R5P was used as the substrate, the Acp production of group C and group T at 60 min was 1.75 mM and 3.79 mM, respectively. The result showed BA-C displayed activity on F6P and R5P, converting them into AcP. However, the activity profile for the BA-C show a higher specificity towards F6P compared to X5P.

3.4. Docking of phosphoketolase with F6P and molecular dynamics simulations to identify catalytic key residues

The crystal structure of phosphoketolase BA-C did not exist in the protein data bank (RCSB PDB). Swiss-Model, the protein structure homology-modelling server was used to construct the protein structure of BA-C, the homologous template was 3AI7, and the identity was 78 %. After the protein structure was constructed, F6P was used as the ligand molecule for molecular docking, and the best conformation of the combination of the two was obtained according to the scoring function (Fig. 4A and B), and the score is 95.019, which is qualified (see Supplementary Data 8). To further investigate the molecular mechanism of protein BA-C binding to F6P, the screened receptor protein-small molecule complex system was then simulated with 100 ns molecular dynamics under npt ensemble, and the trajectory data were saved every 10 ps. According to the RMSD curve analysis, the complex reached dynamic equilibrium at around 20 ns (Fig. 4C and Fig. S7) and finally converged. This indicates that the small molecules are well-matched to the target proteins and can form stable complexes. In addition, RMSF analysis shows that a small part of amino acids in the protein complex changed conformation, while most of the amino acids changed little (Fig. 4D). The binding energy of PK protein and F6P was −118.726 kcal/mol by modeling and fitting. For identifying the key binding sites of phosphoketolase and F6P, all of the contacts that may influence substrate recognition and product release are registered, including hydrogen bonds, hydrophobic interactions, π-stacking, and salt bridges [34]. As a result, a total of 17 individual residues at the pockets were collected. Protein BA-C and F6P can form hydrogen bond interaction, and the interaction residue sites include Thr-67, His-97, Gly-183, and Lys-300 (Fig. 4E). The energy around the residue site was calculated and the energy distribution diagram was obtained (Fig. 4F).

3.5. Alanine scanning mutagenesis to identify effective mutation sites

To identify key amino acid sites to guide site-specific amino acid mutation, we performed alanine scanning mutations on these amino acid residues and replaced relevant amino acid residues with neutral alanine without a special side chain, respectively [50]. These key amino acids might affect the activity of the enzyme, and mutants with a 10 % change in relative enzyme activity were thought to affect catalysis [30]. According to the information on residue sites (Fig. 4F), we carried out alanine mutation at 21 sites respectively. The mutant genes were expressed separately in strain S19 and 21 strains were obtained. These strains were cultured on a 96-well plate with an economizing medium of 2 % galactose and 2 % raffinose pentahydrate, and their biomass was monitored (Fig. S8). The yield of tyrosol was measured after 72 h of culture (Fig. 4G). The data showed that alanine mutations at Gly183Ala, Tyr217Ala, and His320Ala, caused the yield of tyrosol to reach 742.48 mg/L, 703.02 mg/L and 602.21 mg/L respectively (Fig. 4G). The tyrosol yield of these three strains increased by 37.07 %, 29.78 %, and 11.17 %, respectively, compared with the control group. However, the mutations of His64Ala, Trp65Ala, Gly66Ala, Thr67Ala, and His97Ala reduced the production of tyrosol, which was lower than that before the mutation. The results showed that the mutation of these sites would cause the activity of the enzyme to be weakened or even inactivated. In the study of Jing Zhang and Yongjun Liu, the His64, His553, and His97 of phosphoketolase are found to have the function to stabilize the transition states and intermediates, and His64 is a better candidate of B1 catalyst [51,52]. Therefore, His64 might not be suitable for mutation. Other side chains that might restrict space for proper binding and orientation of an acceptor substrate like His320, Asn549, and Tyr501 were found to be crucial for phosphoketolase activity [53,54]. According to the alanine mutations at Gly183Ala, Tyr217Ala, and His320Ala, we speculate that this site may increase the interaction between the enzyme and the substrate.

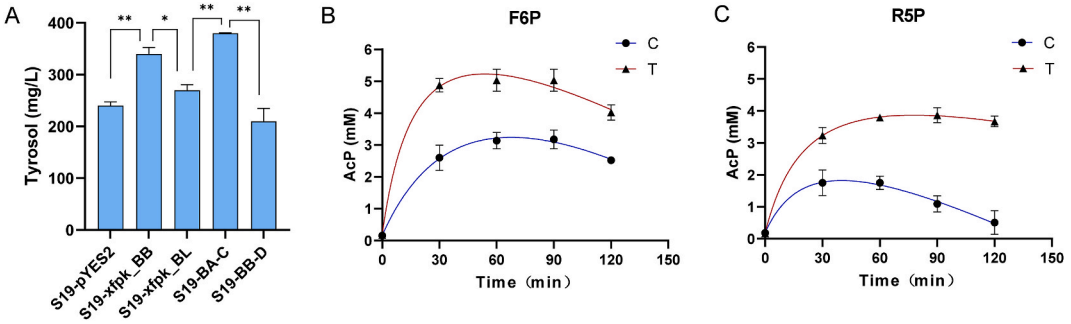

Fig. 3. Activity and substrate specificity of phosphoketease in *S. cerevisiae*. (A) Utilizing galactose as an inducer to express phosphoketolase in *S. cerevisiae*. (B) and (C) *In vitro* enzymatic activity assay to determine the substrate specificity and enzymatic activity of phosphoketolase towards R5P and F6P, respectively. The blue fitted curve (Group C) stands for the crude enzyme extract of S19-pYES2, red fitted curve (Group T) stands for the crude enzyme extract of S19-BA-C.

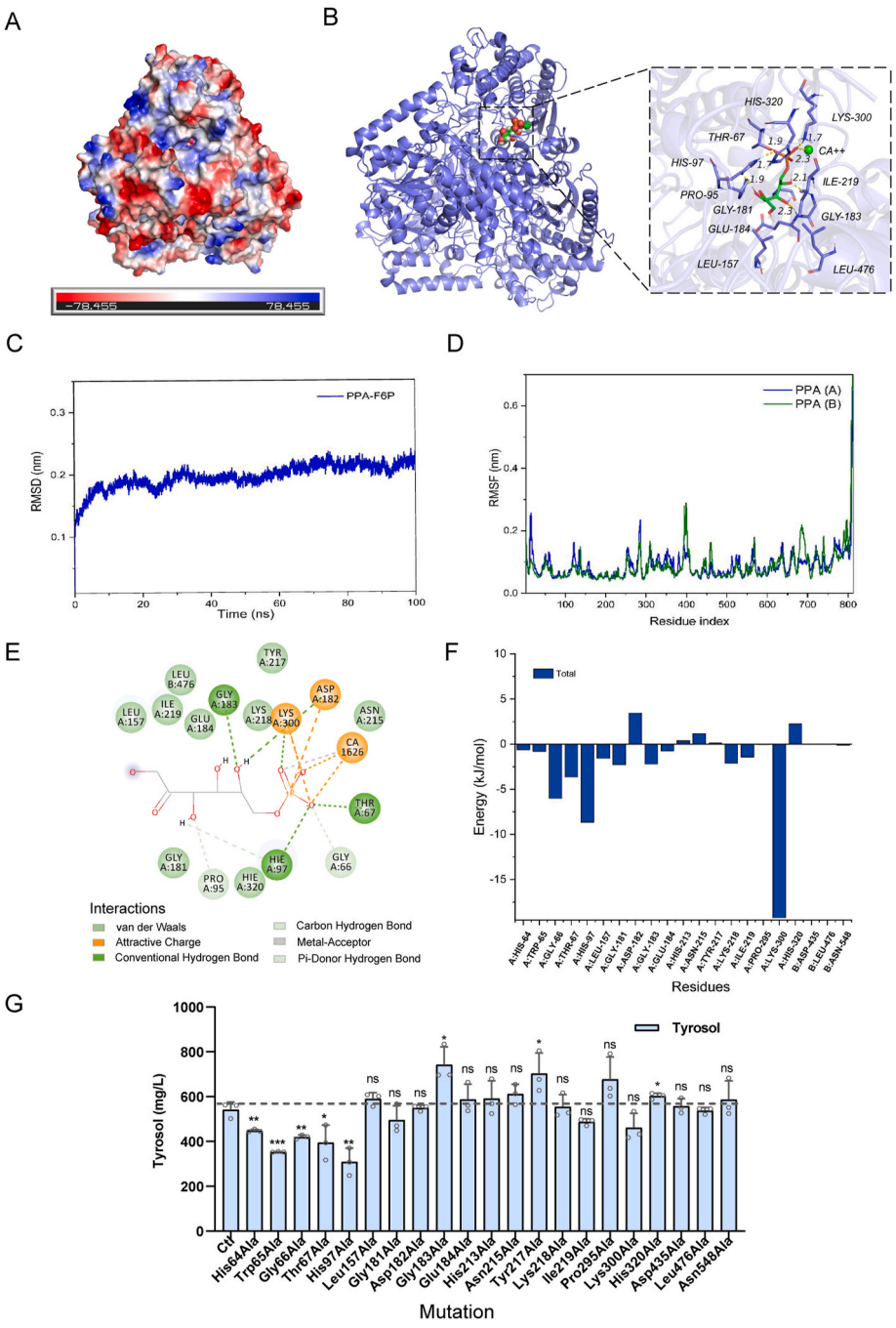

Fig. 4. Results of molecular docking and dynamics simulation. (A) Molecular docking conformation. (B) Interaction between the enzyme and the substrate molecule. (C) RMSD plot, the PPA in the figure represents the abbreviation of phosphoketolase. (D) RMSF plot, PPA (A) and PPA (B) represent the two subunits of the enzyme, respectively. (E) Form of the interaction between phosphoketolase and F6P. (F) Energy profile of amino acid residues. (G) Production of tyrosol after free expression in *S. cerevisiae* S19 following alanine mutation at phosphoketolase residue site.

3.6. Molecular dynamics simulation predicts mutation sites

To further explore the possibility of increasing enzyme activity by mutating these sites, we predicted the effect of saturation mutation scanning at these sites on protein stability by calculation. According to the experimental results, three amino acid sites Gly-183, Tyr-217, and His-320 were selected for mutation prediction, each amino acid was scanned for saturation mutation (20 amino acids), and the affinity for the compound after mutation and the influence of this site on protein stability were calculated. 60 mutation data were obtained from 3 amino acid sites saturated mutation scanning (Fig. 5A and B). We classified the 60 mutation data according to the influence of the mutated amino acids on protein stability and removed the delta stability and delta affinity values greater than 0.5, obtained His320Arg, His320Gln, and His320-Met. Three phosphoketolase mutants BA-C^{His320Arg}, BA-C^{His320Gln}, and BA-C^{His320Met} were obtained by site-directed mutagenesis. The wild-type BA-C and mutants were molecular-docked with F6P. The interaction between BA-C and F6P is mainly hydrogen bonds and carbon-hydrogen bonds (Fig. 5C). Hydrogen bonds include Thr-67, His-97, Gly-183, and Lys-300. The carbon-hydrogen bonds mainly consist of Gly-183, Lys-218, Pro-95, His-97, and Gly-66. The interaction of BA-C^{His320Arg} with F6P increased the hydrogen bond at Pro-95. The interaction of BA-C^{His320Gln} with F6P increased the hydrogen bond at His-97 and Ca^{++} The interaction of BA-C^{His320Gln} with F6P increased the hydrogen bond at

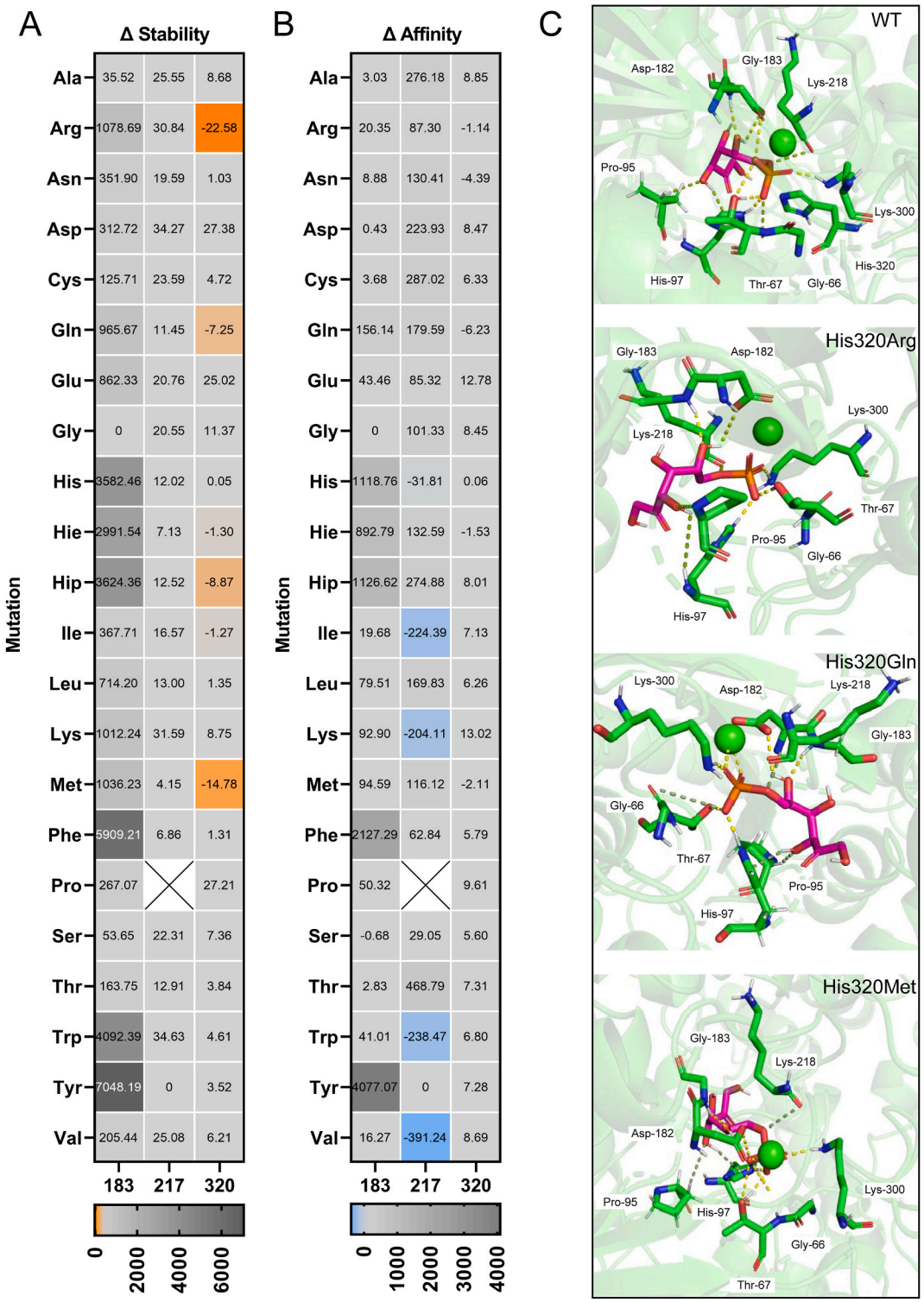

Fig. 5. Mutation prediction and molecular docking after mutation. (A) Stability prediction at sites 183, 217, and 320 mutated into other 20 amino acids. (B) Affinity prediction at sites 183, 217, and 320 mutated to 20 amino acids (Blanks represent missing data.). (C) Molecular docking after mutation of locus 320 into Arg, Gln, and Met (Yellow dotted lines represent hydrogen bonds, green dotted lines represent carbon-hydrogen bonds.).

Gly-66. In addition, we simulated the size of the active pocket of the mutants and the changes in the surrounding hydrogen bond energy. It was found that the entrance channels of the substrate pockets of BA-$C^{His320Arg}$, BA-$C^{His320Gln}$, and BA-$C^{His320Met}$ were larger than those before the mutation, and the increase of the entrance channel was often conducive to the entry of the substrate into the active center (Fig. S9). Based on the results of molecular docking, we hypothesize that an increase in hydrogen bonding enhances the interaction between phosphoketolase and P6P, which together with the increase in substrate channeling leads to an increase in enzyme activity [55].

3.7. Mutation validation and in vitro enzyme activity assay

According to the predicted mutation sites, we carried out

experimental verification. Subsequently, the mutated amino acids were constructed into the pYES2 plasmid expression cassette and expressed in strain S19 to obtain strains S19-320Arg, S19-320Gln, and S19-320Met, and the tyrosol titer reached 772.19 mg/L, 750.98 mg/L, and 826.43 mg/L, respectively. They were separately increased by 42.55 %, 38.64 %, and 52.57 % compared to S19-BA-C (Fig. 6A). In addition, we completed the mutation of the remaining 57 amino acids, and the mutation results were roughly similar to the predicted results, further indicating that site 320 was a key site that played a decisive role in enzyme activity (Fig. S10–12). To be stably expressed in yeast, it was not affected by passage and did not need to be induced by galactose, we added constitutive promoter *TEF1* to the wild and mutated phosphoketolase sequence and integrated them into the locus Chr IV of strain S19 yield S21, S22, S23, and S24. Studies have shown that AcP could be converted to acetic acid, which causes metabolic burden and toxicity to cells. To reduce the production of acetic acid, we knocked out gene *GPP1* encoding a glycerol-3-phosphate dehydrogenase and heterologously expressed the gene *SePTA* from *Salmonella enterica* in strains S21, S22, S23, and S24, and obtained strains S25, S26, S27, and S28 (Figs. 1 and 6B) [27,56]. The operations could not only introduce AcP into the TCA cycle but also eliminate excess acetic acid as a by-product (Fig. S13). The tyrosol titer of S25, S26, S27 and S28 reached 368.63 mg/L, 538.41 mg/L, 524.89 mg/L and 455.57 mg/L, respectively. The mutant strains separately increased by 46.05 %, 42.38 %, and 23.58 % compared to S25. Subsequently, to further explore the changes in its enzyme activity, we measured the amino acid enzyme activity after these mutations. The mutation at locus 320 increased the enzyme activity to different degrees. Mutating 320 His into Met more significantly impacted the phosphoketolase activities toward F6P, and the catalytic efficiency for F6P increased by 37.32 % (k_{cat}/K_m), after mutating 320 His into Arg, the catalytic efficiency for F6P increased by 20.71 % (Table 1). We observed that the phosphoketolase activities of BA-C and its mutants had the following order: 320-Met >320-Arg >320-Gln. However, the mutation did not significantly improve the enzyme activity of R5P.

3.8. Glucose fed-batch fermentation for higher tyrosol production

Fed-batch fermentation was applied to further improve the titer of tyrosol biosynthesized in *S. cerevisiae*. Strain S19, S25, S26, and S27 were selected for the fed-batch fermentation, which was performed in a 20 L bioreactor containing 14 L of the YPD medium. After the depletion of the initial glucose feed (approximately after 9 h), glucose was fed periodically into the bioreactor to control the glucose concentration in the fermentation medium under 5 g/L. As shown in Fig. 7A and Fig. S14A, glucose and ethanol were gradually consumed after 60 h. The cell density (OD_{600}) of strain S19 reached about 23.79, and the tyrosol titer continued to accumulate, eventually reaching 2.09 g/L. The OD_{600} of strain S25 achieved an OD_{600} value of 23.16 after 60 h cultivation and the production of tyrosol reached up to 3.67 g/L (Fig. 7B). In addition, 5.25 g/L and 4.75 g/L tyrosol were produced during the fermentation of strain S26 and S27 after 60 h (Fig. 7C and D). The tyrosol yield of stain S25, S26, and S27 in the fermenter increased by 75.59 %, 151.19 %, and 127.27 %, respectively, compared with stain S19. The tyrosol yield of stain S26 and S27 increased by 43.05 % and 29.43 %, respectively, compared with stain S25.

4. Discussion

In our work, we utilized a metabolic engineering strategy to obtain strain S19 producing 247.66 mg/L of tyrosol, which contained expression of the heterologous *PcAAS* gene, mutations in the feedback repressor genes *ARO3*, *ARO4*, *ARO7,* gene overexpression of *ARO4*^{K229L} and the endogenous gene *ARO10*, as well as knockdown of the gene *PDC1*, *PHA2*, and *TRP2* which participate in competitive pathways. The tyrosol production of this strain was still at a low level compared to the tyrosol production of *S. cerevisiae* constructed by Liu et al. [20]. Tyrosol was de novo synthesized using glucose and was limited by the production of the precursor substance E4P. We construct a strategy based on the phosphoketolase pathway to further increase tyrosol production. Compared to the approach of modifying the endogenous gene *TKL*, *RKL1* in *S. cerevisiae* to increase the carbon flux to E4P, the modification of phosphoketolase alone was more efficient. In this paper, a phosphoketolase with high enzyme activity was screened by mining big data and constructing a phylogenetic tree combined with tyrosol detection. We modified the phosphoketolase BA-C by semi-rational design and obtained the phosphoketolase mutant, which showed high catalytic efficiency for F6P. The molecular docking results further revealed the mechanism of the improvement of BA-C enzyme activity. The increase in the number of hydrogen bonds improves the binding force between the phosphoketolase BA-C and the substrate F6P. In addition, the increased in the entrance channel of the substrate active pocket facilitated F6P to reach the active center. In the end, the strain we constructed increased

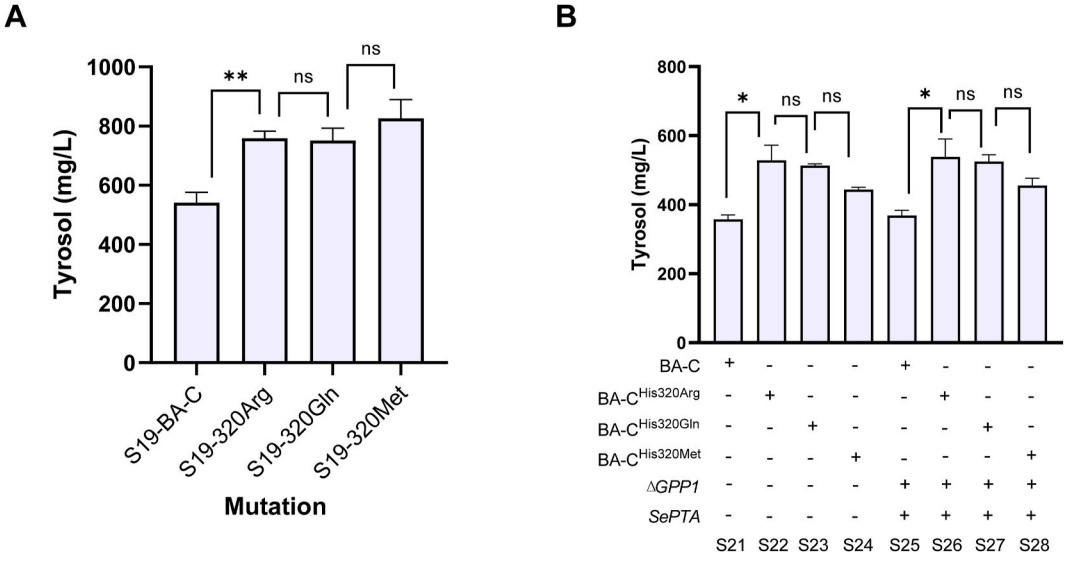

Fig. 6. Production of tyrosol in *S. cerevisiae* S19 after phosphoketolase BA-C mutation. (A) Tyrosol production of *S. cerevisiae* S19 which contained phosphoketolase mutated 320Arg, 320Gln, and 320Met. (B) The 320Arg, 320Gln, and 320Met mutated phosphoketolase genes were inserted into the genome to determine the yield of tyrosol and the production of tyrosol after completing the PHK pathway.

Table 1
Kinetic parameters for phosphoketolases and its mutants using F6P and R5P as substrates.

Enzyme variants	F6P			R5P		
	K_m (μM)	k_{cat} (min^{-1})	k_{cat}/K_m(M^{-1}·min^{-1})	K_m (μM)	k_{cat} (min^{-1})	k_{cat}/K_m (M^{-1}·min^{-1})
WT	15.24	0.003188	209.1863517	16.79	0.003311	197.2007147
320-Arg	21.25	0.005366	252.5176471	16.93	0.003655	215.8889545
320-Gln	21.69	0.004892	225.5417243	23.33	0.004718	202.2288898
320-Met	16.02	0.004599	287.0786517	27.38	0.005355	195.5807159

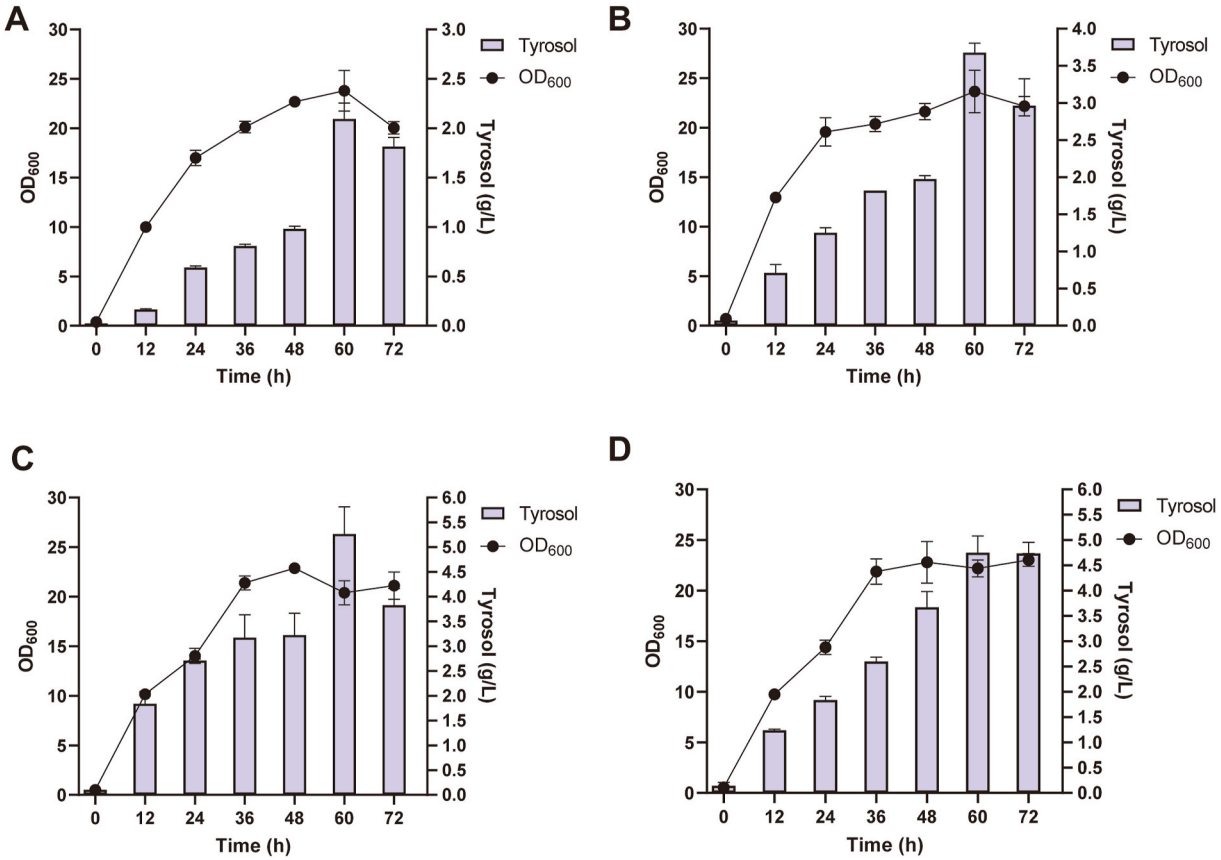

Fig. 7. Tyrosol production of engineered *S. cerevisiae* in a 20 L fermenter. A, B, C, and D correspond to the tyrosol production of strain S19, strain S25, strain S26, and strain S27 respectively, and the methods of fermentation control were consistent.

by 151.19 % compared with the control strain. Although the final yield of tyrosol was still lower than that of the predecessors, the phosphoketolase screened in this paper was more efficient in increasing E4P flux (Table 2).

In the previous strategy of metabolic engineering, feedback inhibition contributed the most to the improvement of tyrosol production, followed by the knockout of competitive pathways. ARO3 had a high binding affinity to L-phenylalanine before mutation, and the interaction with L-phenylalanine was weak after becoming mutant $ARO3^{D154N}$. It greatly alleviated the feedback inhibition caused by L-phenylalanine accumulation. The $ARO4^{K222L}$ mutation located L-tyrosine in the vicinity of the helix α3 and α3/β3 rings, and abolished the inhibitory effect of L-tyrosine on itself [19]. The permutation and combination of *ARO3*, *ARO4,* and *ARO7* mutations have different effects on the production of tyrosol. This highlights the importance of the $ARO4^{K222L}$ mutation, but it is not completely ruled out that it is caused by differences between strains. The throttling of the branching pathway is important, but it is impossible to completely knock out the production of tryptophan or phenylalanine for *S. cerevisiae*. This also explains why the production of tyrosol did not increase after a series of knockdown operations, and there was still a certain amount of production of 2-phenylethanol and tryptophol [41]. Therefore, on this basis, overexpression of phenylalanine-4-hydroxylase (P4H) can be considered to increase the production of tyrosol by converting phenylalanine into tyrosine. However, this strategy has not been studied in *S. cerevisiae*.

Phosphoketolases are members of the thiamine pyrophosphate (TPP)-dependent enzyme family and play a vital role in carbohydrate metabolism in various microorganisms [57]. In our study, BC-A is derived from *Bifidobacterium*. Unlike other organisms, bifidobacteria use a unique carbohydrate metabolic pathway called “bifid shunt”, which can use phosphoketolase to phosphorylate F6P and X5P [47,58]. This function allows bifidobacteria to produce more ATP from carbohydrates than other conventional pathways. However, phosphoketolases found in other organisms (called XPK) are mainly able to metabolize X5P and have very low activity towards F6P [59–62]. In contrast, phosphoketolase derived from *Bifidobacterium* origin has a high activity towards F6P, which is similar to our experimental results. Therefore, through the above research on BC-A, we speculate that the enzyme belongs to the XFPK enzyme.

Phosphoketolase has been gradually applied in cell factories in recent years for the efficient production of *p*-coumaric acid, resveratrol, salidroside, and 2-phenylethanol in yeast by means of carbon flux

Table 2
Summary of recent reports regarding the production of tyrosol from glucose.

Products	Host	Metabolic engineering strategies	Culture conditions	Titer	References
Tyrosol/ salidroside	*S. cerevisiae* BY4742	Integrating with *URA3* selectable marker and P_{PGK1}-*ARO7*^{G141S}-T_{ADH1}-P_{TDH3}-*ARO4*^{K229L}-T_{TEF1}- P_{TEF1}-*AroL*-T_{CYC1} cassettes into *YPRC*Δ15DNA site. Integrating with *LEU2* selectable marker and P_{PGK1}-*AtUGT85A1*$_{syn}$-T_{ADH1}-P_{TDH3}-*PcAAS*$_{syn}$ -T_{TEF1} cassettes into YJR056C DNA site	5 L bioreactor fed-batch fermentation	732.5 mg/L salidroside and 1394.6 mg/L tyrosol	[14]
Tyrosol	*S. cerevisiae* BY4741	pJFE3 carrying P_{TDH3}-*PcAAS*$_{syn}$-T_{CYC1} P_{TEF1}-*EcADH*$_{syn}$-T_{PGK1} cassette, Δ*pdc1* and *EcTyr*$^{AM53I/A354V}$ expressed	Shake flask fermentation	126.74 ± 6.70 mg/g DCW (SC-Ura medium with 2 % glucose)	[13]
Tyrosol/ salidroside	*S. cerevisiae* HLF-Dα	PHA2:P_{TPI1}-*BbXFPK*-T_{GPM1}-loxp- *kanMX4-loxp*, *TRP3*::P_{TEF1}-*UGT85a1*-T_{CYC1}-*hphMX4*	3 L bioreactor	Tyrosol 8.48 g/L and 1.82 g/L salidroside (after 192 h cultivation)	[12]
Tyrosol	*S. cerevisiae* CEN.PK2–1C	*ZWF1*::P_{HXT7}-*TKL1*-T_{ADH1}-P_{TEF1}-*RKI1*-T_{PGK1} *TRP1*,*URA3*::P_{PGK1}-*ARO2*-T_{GPD}-P_{TEF1}-*ARO10*-T_{PGK1} ,Δ*pdc1* Δ*pha2* 308a:P_{ARO4}-*ARO4*^{K229L}-T_{ARO4}-P_{ARO7}-*ARO7*^{G141S}-T_{ARO7}-P_{ARO3}-*ARO3*^{K222L}-T_{ARO3}	Shake flask fermentation	702.30 mg/L	[20]
Tyrosol/ salidroside	*S. cerevisiae* CEN.PK2–1C	*ZWF1*::P_{HXT7}-*TKL1*-T_{ADH1}-P_{TEF1}-*RKI1*-T_{PGK1} *TRP1*,*URA3*::P_{PGK1}-*ARO2*-T_{GPD}-P_{TEF1}-*ARO10*-T_{PGK1} ,Δ*pdc1* Δ*pha2* 308a:P_{ARO4}-*ARO4*^{K229L}-T_{ARO4}-P_{ARO7}-*ARO7*^{G141S}-T_{ARO7}-P_{ARO3}-*ARO3*^{K222L}-T_{ARO3},*LEU2*::P_{TEF1}-*RrU8GT33*^{opt}-T_{PGK1}	5 L bioreactor	9.90 g/L of tyrosol and 26.55 g/L of salidroside	[20]
Tyrosol	*S. cerevisiae* CEN.PK2–1C	308a:P_{TDH3}-*ARO4*^{K229L}-T_{FBA1}-P_{TEF2}-*ARO7*^{G141S}-T_{ADH2},Δ*pdc1*Δ*pha2*, *URA3*::P_{PGK1}-*ARO2*-T_{GPD}-P_{CCW12}-*ARO10*-T_{ADH1}, *TRP1*::P_{HXT7}-*TKL1*-T_{ADH1}-P_{TEF1}-*RKI1*-T_{PGK1}, *LEU2*::P_{TEF1}-*ARO3*^{D154N}-T_{PGK1t}	Shake flask fermentation	1.3 g/L of tyrosol	[19]

redistribution [12,63,64]. In addition, the enzyme has been applied to increase cellular fatness and product yields in *Pseudomonas putida* through an engineered phosphoketolase shunt [49]. Generalist phosphoketolase Xfspk is used to convert glucose into stoichiometric amounts of AcP for improving the carbon yield of *E. coli*. These studies indicate that the excavation of phosphoketolase will be beneficial to the biosynthesis of compounds.

To obtain higher-activity phosphoketolase, Dele-Osibanjo et al. screened live high-activity phosphoketolase PKT$^{T2A/I6T/H260Y}$ by directed evolution [47]. The results showed that compared with a single amino acid mutation, the mutation of the three amino acid sites resulted in a greater increase in enzyme activity. This result inspires us need to combine multiple amino acid mutations and then determine the effect on enzyme activity and tyrosol. Different from directed evolution, we obtained the 320 key amino acid residues and mutant amino His320Arg by semi-rational design. The mutation increased the activity of the enzyme to F6P (37.32 %) and R5P. The mutation sites obtained by directed evolution are far away from the active center. However, the activity of the enzyme was also improved. This leads us to believe that there may be great potential regarding amino acid mutations. Further molecular docking of the phosphoketolase to R5P could be done to explain the effect of the mutation on the binding of R5P and the differential binding with F6P. According to our experimental results, the His320Arg amino acid mutation increases the number of hydrogen bonds and increases the space size of the substrate channel. Hydrogen bond is the main interaction force maintaining the stability of the α-helical structure. Mutated His320Arg formed an additional hydrogen bond with Pro-95, making BA-C a tighter structure for improved catalytic activity. In addition, the size of the substrate channel determines the efficiency of the substrate entering the enzyme activity region, which may lead to an increase in enzyme activity.

Algorithm-based calculation of virtual mutation provides the direction of mutation, but its accuracy is not as high, so further validation using traditional wet experiments is needed. In addition, there is currently less crystal structure information related to phosphoketolase [65]. With the development of technology, the publication of more structural information will play an important role in the mining of phosphoketolase. However, within the scope of the prior art, structure-guided protein rational design and directed enzyme evolution are still successful proven approaches in engineering and improving enzyme properties.

5. Conclusion

We excavated and identified the XFPK enzyme BA-C, analyzed its structural characteristics, and the difference in substrate activity of the enzyme. After the enzyme was applied to the final fermentation, the yield of tyrosol was increased by 151.19 %. This further illustrates that the development of phosphoketolase will provide strong support for the improvement of aromatic and other de novo synthetic compounds.

CRediT authorship contribution statement

Na Song: Writing – review & editing, Writing – original draft, Visualization, Validation, Supervision, Software, Resources, Project administration, Methodology, Investigation, Formal analysis, Data curation, Conceptualization. **Huili Xia:** Writing – review & editing, Writing – original draft, Visualization, Validation, Supervision, Software, Resources, Project administration, Methodology, Investigation, Formal analysis, Data curation, Conceptualization. **Yaoru Xie:** Data curation. **Shuaikang Guo:** Data curation. **Rong Zhou:** Writing – original draft. **Lingling Shangguan:** Writing – original draft. **Kun Zhuang:** Writing – original draft. **Huiyan Zhang:** Data curation, Conceptualization. **Feiran An:** Data curation, Conceptualization. **Xueyun Zheng:** Writing – review & editing. **Lan Yao:** Writing – review & editing. **Shihui Yang:** Writing – review & editing. **Xiong Chen:** Resources, Funding acquisition. **Jun Dai:** Resources, Funding acquisition.

Declaration of competing interest

Authors declare that this manuscript is original and authors have no known conflict of interest associated with this manuscript. We have not excluded any individual who satisfied the authorship criteria. We confirm that all of the listed authors have read and approved the content of the manuscript.

Acknowledgments

This work was supported by the National Natural Science Foundations of China (Grant Nos. 31871789 and 41876114), the key project of Hubei Provincial Department of Education (T2022011), the Natural Science Foundation of Hubei Province (No. 2024AFB803).

Appendix. A Supplementary data

Supplementary data to this article can be found online at https://doi.org/10.1016/j.synbio.2024.11.007.

References

[1] Kim YY, Lee S, Kim MJ, Kang BC, Dhakal H, Choi YA, et al. Tyrosol attenuates lipopolysaccharide-induced acute lung injury by inhibiting the inflammatory response and maintaining the alveolar capillary barrier. Food Chem Toxicol 2017; 109Pt 1:526–33.

[2] St-Laurent-Thibault C, Arseneault M, Longpré F, Ramassamy C. Tyrosol and hydroxytyrosol, two main components of olive oil, protect N2a cells against amyloid-β-induced toxicity. Involvement of the NF-κB signaling. Curr Alzheimer Res 2011;85:543–51.

[3] Satoh Y, Tajima K, Munekata M, Keasling JD, Lee TS. Engineering of a tyrosol-producing pathway, utilizing simple sugar and the central metabolic tyrosine, in *Escherichia coli*. J Agric Food Chem 2012;604:979–84.

[4] Torrens-Spence MP, Pluskal T, Li FS, Carballo V, Weng JK. Complete pathway elucidation and heterologous reconstitution of *Rhodiola* salidroside biosynthesis. Mol Plant 2018;111:205–17.

[5] Li X, Chen Z, Wu Y, Yan Y, Sun X, Yuan Q. Establishing an artificial pathway for efficient biosynthesis of hydroxytyrosol. ACS Synth Biol 2018;72:647–54.

[6] Mao Y, Li Y, Yao N. Simultaneous determination of salidroside and tyrosol in extracts of *Rhodiola L.* by microwave assisted extraction and high-performance liquid chromatography. J Pharm Biomed Anal 2007;453:510–5.

[7] Flourat AL, Combes J, Bailly-Maitre-Grand C, Magnien K, Haudrechy A, Renault JH, et al. Accessing *p*-hydroxycinnamic acids: chemical synthesis, biomass recovery, or engineered microbial production? ChemSusChem 2021;141:118–29.

[8] Woodburn HM, Stuntz CF. The synthesis of β-(3-Amino-4-hydroxyphenyl)-ethanol; 3-aminotyrosol. Am Chem Soc 1950;72:1361–4.

[9] Yamada S-i, Fujii T, Takagi K, Gomi Y, Matsushita S. Preparation of tyrosol and 4-Methoxyphenethyl alcohol. Chem Pharm Bull 1963;11:258–60.

[10] Chung D, Kim SY, Ahn JH. Production of three phenylethanoids, tyrosol, hydroxytyrosol, and salidroside, using plant genes expressing in *Escherichia coli*. Sci Rep 2017;71:2578.

[11] Yang H, Xue Y, Yang C, Shen W, Fan Y, Chen X. Modular engineering of tyrosol production in *Escherichia coli*. J Agric Food Chem 2019;6714:3900–8.

[12] Guo W, Huang Q, Feng Y, Tan T, Niu S, Hou S, et al. Rewiring central carbon metabolism for tyrosol and salidroside production in *Saccharomyces cerevisiae*. Biotechnol Bioeng 2020;1178:2410–9.

[13] Guo W, Huang Q, Liu H, Hou S, Niu S, Jiang Y, et al. Rational engineering of chorismate-related pathways in *Saccharomyces cerevisiae* for improving tyrosol production. Front Bioeng Biotechnol 2019;7:152.

[14] Jiang J, Yin H, Wang S, Zhuang Y, Liu S, Liu T, et al. Metabolic engineering of *Saccharomyces cerevisiae* for high-level production of salidroside from glucose. J Agric Food Chem 2018;6617:4431–8.

[15] Nielsen J. Yeast systems biology: model organism and cell factory. Biotechnol J 2019;149:e1800421.

[16] Borodina I, Nielsen J. Advances in metabolic engineering of yeast *Saccharomyces cerevisiae* for production of chemicals. Biotechnol J 2014;95:609–20.

[17] Hazelwood LA, Daran JM, van Maris AJ, Pronk JT, Dickinson JR. The Ehrlich pathway for fusel alcohol production: a century of research on *Saccharomyces cerevisiae* metabolism. Appl Environ Microbiol 2008;748:2259–66.

[18] Liu Q, Yu T, Li X, Chen Y, Campbell K, Nielsen J, et al. Rewiring carbon metabolism in yeast for high level production of aromatic chemicals. Nat Commun 2019;101: 4976.

[19] Liu H, Xiao Q, Wu X, Ma H, Li J, Guo X, et al. Mechanistic investigation of a D to N mutation in DAHP synthase that dictates carbon flux into the shikimate pathway in yeast. Commun Chem 2023;61:152.

[20] Liu H, Tian Y, Zhou Y, Kan Y, Wu T, Xiao W, et al. Multi-modular engineering of *Saccharomyces cerevisiae* for high-titre production of tyrosol and salidroside. Microb Biotechnol 2021;146:2605–16.

[21] Paravicini G, Schmidheini T, Braus G. Purification and properties of the 3-deoxy-D-arabino-heptulosonate-7-phosphate synthase (phenylalanine-inhibitable) of *Saccharomyces cerevisiae*. Eur J Biochem 1989;1861–2:361–6.

[22] Schnappauf G, Hartmann M, Künzler M, Braus GH. The two 3-deoxy-D-arabino-heptulosonate-7-phosphate synthase isoenzymes from *Saccharomyces cerevisiae* show different kinetic modes of inhibition. Arch Microbiol 1998;1696:517–24.

[23] Liu H, Wu X, Ma H, Li J, Liu Z, Guo X, et al. High-Level production of hydroxytyrosol in engineered *Saccharomyces cerevisiae*. ACS Synth Biol 2022;1111: 3706–13.

[24] Suástegui M, Yu Ng C, Chowdhury A, Sun W, Cao M, House E, et al. Multilevel engineering of the upstream module of aromatic amino acid biosynthesis in *Saccharomyces cerevisiae* for high production of polymer and drug precursors. Metab Eng 2017;42:134–44.

[25] Gold ND, Gowen CM, Lussier FX, Cautha SC, Mahadevan R, Martin VJ. Metabolic engineering of a tyrosine-overproducing yeast platform using targeted metabolomics. Microb Cell Factories 2015;14:73.

[26] Bergman A, Hellgren J, Moritz T, Siewers V, Nielsen J, Chen Y. Heterologous phosphoketolase expression redirects flux towards acetate, perturbs sugar phosphate pools and increases respiratory demand in *Saccharomyces cerevisiae*. Microb Cell Factories 2019;181:25.

[27] Bergman A, Siewers V, Nielsen J, Chen Y. Functional expression and evaluation of heterologous phosphoketolases in *Saccharomyces cerevisiae*. Amb Express 2016;61: 115.

[28] Chen S, Xu Z, Ding B, Zhang Y, Liu S, Cai C, et al. Big data mining, rational modification, and ancestral sequence reconstruction inferred multiple xylose isomerases for biorefinery. Sci Adv 2023;95:eadd8835.

[29] Abramson J, Adler J, Dunger J, Evans R, Green T, Pritzel A, et al. Accurate structure prediction of biomolecular interactions with AlphaFold 3. Nature 2024; 6308016:493–500.

[30] Liu L, Zhou S, Deng Y. Rational design of the substrate tunnel of β-ketothiolase reveals a local cationic domain modulated rule that improves the efficiency of claisen condensation. ACS Catal 2023;1312:8183–94.

[31] Zhou A, Zhou K, Li Y. Rational design strategies for functional reconstitution of plant cytochrome P450s in microbial systems. Curr Opin Plant Biol 2021;60: 102005.

[32] Li JK, Qu G, Li X, Tian Y, Cui C, Zhang FG, et al. Rational enzyme design for enabling biocatalytic *Baldwin* cyclization and asymmetric synthesis of chiral heterocycles. Nat Commun 2022;131:7813.

[33] Xu H, Yu B, Wei W, Chen X, Gao C, Liu J, et al. Improving tyrosol production efficiency through shortening the allosteric signal transmission distance of pyruvate decarboxylase. Appl Microbiol Biotechnol 2023;10711:3535–49.

[34] Qu G, Liu B, Zhang K, Jiang Y, Guo J, Wang R, et al. Computer-assisted engineering of the catalytic activity of a carboxylic acid reductase. J Biotechnol 2019;306: 97–104.

[35] Tamura K, Stecher G, Kumar S. MEGA11: molecular evolutionary genetics analysis version 11. Mol Biol Evol 2021;387:3022–7.

[36] Wang Q, Xu J, Sun Z, Luan Y, Li Y, Wang J, et al. Engineering an in vivo EP-bifido pathway in *Escherichia coli* for high-yield acetyl-CoA generation with low CO(2) emission. Metab Eng 2019;51:79–87.

[37] Laughery MF, Wyrick JJ. Simple CRISPR-cas9 genome editing in *Saccharomyces cerevisiae*. Curr Protoc Mol Biol 2019;1291:e110.

[38] Labun K, Montague TG, Gagnon JA, Thyme SB, Valen E. CHOPCHOP v2: a web tool for the next generation of CRISPR genome engineering. Nucleic Acids Res 2016; 44W1:W272–6.

[39] Gietz RD, Schiestl RH. High-efficiency yeast transformation using the LiAc/SS carrier DNA/PEG method. Nat Protoc 2007;21:31–4.

[40] Baek S, Utomo JC, Lee JY, Dalal K, Yoon YJ, Ro DK. The yeast platform engineered for synthetic gRNA-landing pads enables multiple gene integrations by a single gRNA/Cas9 system. Metab Eng 2021;64:111–21.

[41] Bisquert R, Planells-Carcel A, Valera-Garcia E, Guillamon JM, Muniz-Calvo S. Metabolic engineering of *Saccharomyces cerevisiae* for hydroxytyrosol overproduction directly from glucose. Microb Biotechnol 2022;155:1499–510.

[42] Künzler M, Paravicini G, Egli CM, Irniger S, Braus GH. Cloning, primary structure and regulation of the ARO4 gene, encoding the tyrosine-inhibited 3-deoxy-D-arabino-heptulosonate-7-phosphate synthase from *Saccharomyces cerevisiae*. Gene 1992;1131:67–74.

[43] Helmstaedt K, Strittmatter A, Lipscomb WN, Braus GH. Evolution of 3-deoxy-D-arabino-heptulosonate-7-phosphate synthase-encoding genes in the yeast *Saccharomyces cerevisiae*. Proc Natl Acad Sci U S A 2005;10228:9784–9.

[44] Steyer D, Ambroset C, Brion C, Claudel P, Delobel P, Sanchez I, et al. QTL mapping of the production of wine aroma compounds by yeast. BMC Genom 2012;13:573.

[45] Wang D, Wang L, Hou L, Deng X, Gao Q, Gao N. Metabolic engineering of *Saccharomyces cerevisiae* for accumulating pyruvic acid. Ann Microbiol 2015;654: 2323–31.

[46] Brochado AR, Matos C, Møller BL, Hansen J, Mortensen UH, Patil KR. Improved vanillin production in baker's yeast through in silico design. Microb Cell Factories 2010;9:84.

[47] Gupta RS, Nanda A, Khadka B. Novel molecular, structural and evolutionary characteristics of the phosphoketolases from *bifidobacteria* and *Coriobacteriales*. PLoS One 2017;122:e0172176.

[48] Yang Y, Liu Y, Zhao H, Liu D, Zhang J, Cheng J, et al. Construction of an artificial phosphoketolase pathway that efficiently catabolizes multiple carbon sources to acetyl-CoA. PLoS Biol 2023;219:e3002285.

[49] Bruinsma L, Martin-Pascual M, Kurnia K, Tack M, Hendriks S, van Kranenburg R, et al. Increasing cellular fitness and product yields in *Pseudomonas putida* through an engineered phosphoketolase shunt. Microb Cell Factories 2023;221:14.

[50] Li L, Ye L, Lin Y, Zhang W, Liao X, Liang S. Enhancing the substrate tolerance of DszC by a combination of alanine scanning and site-directed saturation mutagenesis. J Ind Microbiol Biotechnol 2020;474–5:395–402.

[51] Scheidig Horvath, SjjoS Biology. Crystal structure of a xylulose 5-phosphate phosphoketolase. Insights into the substrate specificity for xylulose 5-phosphate. 2019.

[52] Zhang J, Liu Y. Computational studies on the catalytic mechanism of phosphoketolase. Computational and Theoretical Chemistry 2013;1025:1–7.

[53] Libuda F. Phosphoketolase - a mechanistic update. In: Department of molecular structural biology. Göttingen: University; 2018. p. 141.

[54] Suzuki R, Katayama T, Kim BJ, Wakagi T, Shoun H, Ashida H, et al. Crystal structures of phosphoketolase, vol. 28544; 2010. p. 34279–87.

[55] Nakata K, Miyazaki N, Yamaguchi H, Hirose M, Kashiwagi T, Kutumbarao NHV, et al. High-resolution structure of phosphoketolase from *Bifidobacterium longum* determined by cryo-EM single-particle analysis. J Struct Biol 2022;2142:107842.

[56] Dai Z, Huang M, Chen Y, Siewers V, Nielsen J. Global rewiring of cellular metabolism renders *Saccharomyces cerevisiae* Crabtree negative. Nat Commun 2018;91:3059.

[57] Rohr LM, Teuber M, Meile L. Phosphoketolase, a neglected enzyme of microbial carbohydrate metabolism. Food Technol 2002;56:270–3.

[58] Stincone A, Prigione A, Cramer T, Wamelink MM, Campbell K, Cheung E, et al. The return of metabolism: biochemistry and physiology of the pentose phosphate pathway. Biol Rev Camb Phil Soc 2015;903:927–63.
[59] Sánchez B, Zúñiga M, González-Candelas F, de los Reyes-Gavilán CG, Margolles A. Bacterial and eukaryotic phosphoketolases: phylogeny, distribution and evolution. J Mol Microbiol Biotechnol 2010;181:37–51.
[60] Suzuki R, Katayama T, Kim BJ, Wakagi T, Shoun H, Ashida H, et al. Crystal structures of phosphoketolase: thiamine diphosphate-dependent dehydration mechanism. J Biol Chem 2010;28544:34279–87.
[61] Glenn K, Smith KS. Allosteric regulation of *Lactobacillus plantarum* xylulose 5-phosphate/fructose 6-phosphate phosphoketolase (Xfp). J Bacteriol 2015;1977:1157–63.
[62] Xiong W, Lee TC, Rommelfanger S, Gjersing E, Cano M, Maness PC, et al. Phosphoketolase pathway contributes to carbon metabolism in cyanobacteria. Nat Plants 2015;2:15187.
[63] Liu M, Wang C, Ren X, Gao S, Yu S, Zhou J. Remodelling metabolism for high-level resveratrol production in *Yarrowia lipolytica*. Bioresour Technol 2022;365:128178.
[64] Hassing EJ, de Groot PA, Marquenie VR, Pronk JT, Daran JG. Connecting central carbon and aromatic amino acid metabolisms to improve de novo 2-phenylethanol production in *Saccharomyces cerevisiae*. Metab Eng 2019;56:165–80.
[65] Nakata K, Kashiwagi T, Kunishima N, Naitow H, Matsuura Y, Miyano H, et al. Ambient temperature structure of phosphoketolase from *Bifidobacterium longum* determined by serial femtosecond X-ray crystallography. Acta Crystallogr D Struct Biol 2023;79Pt 4:290–303.